Band engineering in silicide alloys

Alexander Slepko and Alexander A. Demkov

Phys. Rev. B **85**, 035311 — Published 12 January 2012

DOI: 10.1103/PhysRevB.85.035311

Band engineering in silicide alloys

Alexander Slepko and Alexander A. Demkov[1]
Department of Physics, The University of Texas at Austin, Austin, Texas 78712, USA

A relatively low conductivity of PtSi is one of the impediments to its application as a contact material in semiconductor technology. In this paper we discuss a possible strategy to control the conductivity of PtSi by manipulating the density of states at the Fermi level through alloying. Using density functional theory, we demonstrate theoretically that alloying PtSi with Ti substantially increases the number of conducting electrons, and suggest possible ways to increase the Ti solubility limit. We identify a tertiary compound with the conducting electron concentration almost three times larger than that of bulk PtSi. We analyze the effect of Ti alloying on the work function of PtSi, and its Schottky barrier height to Si and we examine the effect of alloy scattering on PtSi conductivity.

I. Introduction

Continuous scaling of complementary metal oxide semiconductor devices drives the search for new metal silicide contact materials to the source, drain and gate of a field effect transistor [1]. Typically, monosilicides are preferred over higher order silicides, such as disilicides, due to a lower Si consumption. Nickel and platinum monosilicides have recently attracted significant interest [2,3]. Metal silicides are formed by a heat treatment of a metal-semiconductor contact. Owing to the formation mechanism silicide-silicon interfaces are essentially free of contamination. Contacts formed in this manner generally show stable electrical characteristics, such as low line and contact resistance, and exhibit excellent mechanical adhesion [4]. Most important, however, is that the use of metal silicides allows the formation of self-aligning contacts whereas in metallic conductors their precise location usually depends on the fabrication process.

In this paper, using PtSi as an example, we employ first principles calculations to identify a strategy of improving electrical properties of silicide alloys *via* band engineering. The electronic structure and elastic constants of PtSi and Pt_2Si have been previously investigated theoretically using density functional theory (DFT) [5-7]. Our group has reported theoretical studies of the surface energy and work function of bulk PtSi [8] and the electronic, optical and surface properties of PtSi thin films [9]. PtSi is attractive because of its relatively low (0.2 eV) Schottky barrier to the valence band of Si (001) and excellent thermal stability [10]. However, as a contact material PtSi suffers from relatively low conductivity (*e.g.* when compared with Pt), which can be traced to the low electronic density of states (DOS) at the Fermi level in bulk PtSi. A look at the PtSi

[1] demkov@physics.utexas.edu

density of states (Fig. 1) reveals that the Fermi level "misses" the high density of states region corresponding to Pt d-states. A naïve integration of the electronic DOS suggests that in a unit cell of bulk PtSi about 7.5 electrons need to be removed in order to shift the Fermi level down in energy towards the high DOS region of the spectrum. To achieve this we suggest doping PtSi with Ti substitutionally on the Pt site. Both PtSi and TiSi monosilicides can be stabilized in a primitive orthorhombic structure with space group Pnma (*#62 in the International X-Ray Tables*) where PtSi crystallizes in a MnP-type lattice and TiSi in a FeB-type lattice shown in Figs. 2a) and 2b), respectively. Moreover, Ti and Pt atoms are almost equal in size (the atomic radius of Ti of 1.4Å is only 5% larger than that of Pt) but Ti contributes only four electrons per atom to the total amount of valence electrons, versus ten contributed by Pt. In a primitive unit cell of PtSi this means that 1.25 out of four Pt-atoms need to be replaced by titanium. We test this idea by the means of first principles DFT calculations. Our calculations suggest that Ti doping may result in a significant increase of the DOS at the Fermi level followed by an increase in the number of conducting electrons (those in the interval $-k_BT + E_F \le E \le k_BT + E_F$). We predict an increase of up to 2.7 times in the number of conducting electrons compared to bulk PtSi. Importantly, we find that on average the Schottky barrier to Si is rather insensitive to Ti doping. Using a simple ideal mixture theory to estimate the entropic effect of mixing, we find the solubility limit of Ti in bulk PtSi (on the Pt-site) at 500K to be ~0.5%. Unfortunately, this is not sufficient to realize the gains in the electron density in practice. To circumvent this problem, we find that additional alloying with gallium or aluminum can significantly increase the solubility limit of Ti in PtSi. We also estimate the effect of alloy scattering on the conductivity.

The rest of the paper is organized as follows. First, we summarize computational details in section II. In section III we discuss the electronic structure of $Ti_xPt_{1-x}Si$ alloys, estimate the carrier density and analyze the effect of Ti doping on the work function and Schottky barrier height with Si (001). Using the Boltzmann transport formalism we calculate the change in conductivity due to the introduced Ti impurity scattering. In Section IV we discuss the solubility limit of Ti in bulk PtSi, and consider possible routes to increase the solubility limit of Ti *via* stabilizing $Ti_xPt_{1-x}Si$ alloys by additional doping with boron, carbon, gallium and aluminum.

II. Computational details

All calculations are done using density functional theory within the local density approximation and ultra-soft pseudopotentials [12] as included in the VASP code [13-17]. We use the valence configurations ($3d^3$, $4s^1$) for titanium, ($6s^1$, $5d^9$) for platinum, and ($3s^2$, $3p^2$) for silicon. The 300 eV kinetic energy cut-off yields 1 meV/cell convergence for bulk PtSi. To investigate the effects of doping with Ti on the DOS and number of carriers at the Fermi level for different Ti concentrations, we consider 2×2×6, 2×2×3, 2×2×2, 2×1×2, 1×2×2 supercells and the primitive cell. For the Brillouin zone

integration of these cells we use the following Monkhorst-Pack [18] k-point meshes: 4×4×2, 4×4×4, 4×4×6, 8×14×12, 14×8×12 and 13×13×17. All structures are optimized with respect to the ionic positions, cell shape and volume until the forces on all atoms are less than 20meV/Å. The energy is converged to 10^{-3} meV/cell. The relaxation is not constrained by symmetry.

We consider $Ti_xPt_{1-x}Si$ and Ti_xPtSi_{1-x} alloys with 0.52%, 1.04%, 1.56%, 3.13%, 6.25% and 12.5% (atomic percent) Ti substitution. For the two lowest concentrations we use the 2×2×6 and 2×2×3 supercells of PtSi (in each case we replace only one Pt atom by Ti). We use a 2×2×2 supercell of PtSi for the Ti concentrations 1.56% and 3.13% where one and two out of the 32 Pt atoms are substituted by Ti. We analyze all 31 different possibilities to substitute two Pt atoms by Ti (3.13%). Alloys with 6.25% Ti can be realized using 2×2×2 supercells of PtSi where four Pt atoms are substituted by Ti. That yields 465 possibilities to arrange the Ti atoms in the cell. In the case of 12.5% Ti (eight atoms in a 2×2×2 supercell) there are 2629575 different possibilities. As such a large number of different calculations is not realizable, in the case of 6.25% of Ti we analyze smaller 2×1×2 and 1×2×2 supercells. In each case that yields 15 structures with the Ti concentration of 6.25% (including symmetrically equivalent structures). In alloys with 12.5% Ti we limit our studies to a primitive cell of PtSi and replace one Pt atom by Ti resulting in only one possible structure. For this high concentration one in principle, could use a bigger simulation cell with a quasi-random distribution of Ti, however, as it turns out the solubility limit makes this case difficult to realize in practice. To calculate the work function and Schottky barrier height, we use slab geometry with simulation cells of the size ~10Å×~10Å×~45Å (the side lengths vary slightly depending on the used models as is described later) along with a 4×4×2 Monkhorst-Pack k-point mesh for the Brillouin zone integration.

III. Electronic and thermodynamic properties of $Ti_xPt_{1-x}Si$ alloys

Influence of Ti doping on the density of states

The high density of states at the Fermi level and is one of the main requirements for having high electrical conductivity. By integrating the DOS within the $2k_BT$ energy window around the Fermi level (*e.g.* at T=300K) the carrier density n can be determined. To analyze the effect of Ti doping on the DOS and n we consider Ti concentration of 0.52%, 1.04%, 1.56%, 3.13%, 6.25% and 12.5%. For concentrations of 3.13% and 6.25% we consider sixty one possible Pt substitutions in total. However, here we only focus on the most stable configurations. Our results for the DOS at the Fermi level and the carrier density n are summarized in Table 1. For comparison, we have included the results for Ti substitution of Si. As expected, in this case the effect on the carrier concentration is minimal. In Figure 3 we show the DOS of $Ti_xPt_{1-x}Si$ for the Ti concentrations 1.56%, 3.13%, 6.25% and 12.5%. Contrary to our original intention to shift the Fermi level

towards the region of high density of Pt d-states we find that it actually moves very little, yet producing a noticeable change in the number of states at the Fermi level! Figure 4 (the partial DOS of the alloy with 12.5% Ti) shows that the increase is due to the introduction of Ti d-states that appear right above the d-states of Pt in energy (the energy difference of the atomic d-levels is $E_{Ti\text{-}d}$-$E_{Pt\text{-}d} \approx 5.42$eV [19]), rather than to a shift of the Fermi energy. Therefore, though the "rigid band" assumption has proven to be an oversimplification, we find that doping with Ti indeed increases the number of carriers in PtSi. We also find that substituting Si by Ti does not affect the carrier concentration. Later we shall analyze the thermodynamic stability of Si-substituted and Pt-substituted TiPtSi alloys.

Influence of Ti doping on the work function and Schottky barrier height

One of the key characteristics of any contact material is its Schottky barrier height (SBH) to Si. Thus it is important to understand how Ti doping may affect the barrier height. We start by considering the effect of doping on the work function (WF) φ_m of PtSi which is defined as a difference between the vacuum energy in the immediate vicinity of its surface and the Fermi level. To simulate the silicide surface we use slab geometry. The thickness of the $Ti_xPt_{1-x}Si$ slab is approximately 25Å and it is followed by 15Å of vacuum to minimize the slab-slab interaction introduced through the periodic boundary conditions. We calculate the local electrostatic potential of the cell, and average it over the x-y plane along the z axis (direction normal to the surface). A typical plot of this planar averaged local potential is shown in Fig. 5 a). We approximate the vacuum energy level with the value of the electrostatic potential in the vacuum region of the simulation cell. The WF is then easily extracted. We compare the WF of $Ti_xPt_{1-x}Si$ with 3.13% Ti (Ti on Pt-site) to bulk PtSi for the surface orientations (001), (010), (100), (101), (011) and (110). We consider three different surface terminations (Pt, Si and Ti termination) as depicted in Figure 6 for the (100) surface. For the (001) orientation a stoichiometric surface is constructed as cleaving in this direction always yields a surface with an equal amount of Pt and Si in the surface plane rather than Pt or Si rumpling out of it (as is the case for all other orientations). Our results are summarized in Table 3 and plotted in Fig. 7. Firstly, we note that with the exception of the Si-terminated (010) surface, Ti slightly increases the WF compared to equivalent PtSi surfaces. Secondly, with the exception of the (101) orientation, Ti-terminated surfaces always have a lower WF than PtSi surfaces with the same orientation and any termination. The highest difference of 0.45eV is found for the (010) surface when comparing the Ti-terminated $Ti_xPt_{1-x}Si$ with Pt-terminated PtSi. This can be traced to Ti 3d states being higher in energy than the d states of Pt. Within the Schottky model, these changes in the WF should greatly influence the barrier height between the metal's Fermi level and the semiconductor's valence or conduction bands. In the following we analyze two theoretical silicide/Si interface models to gain insight in the dependence of the SBH on Ti doping.

The Schottky barrier height (SBH) of a metal to a p-type semiconductor is defined as the energy difference between the top of the valence band of the semiconductor and the Fermi level of the metal:

$$\varphi_p = E_{VB} - \varphi_m , \qquad (1)$$

where E_{VB} is the energy of the semiconductor's valence band top with respect to the vacuum level, and φ_m is the metal WF. Conversely, the n-type SBH is the energy difference between the Fermi level of the metal and the bottom of the conduction band of the semiconductor.

To estimate the effect of Ti doping on the SBH we construct two model interfaces Si(001)/Ti_xPt_{1-x}Si(001) and Si(001)/Ti_xPt_{1-x}Si(110) using superlattice geometry. We calculate the SBH for 0% and 3.13% Ti, while substituting Ti at the interface directly as that yields the largest change in the WF. The ~35Å thick Si slab is used as a substrate, *i.e.* the silicide layers are laterally lattice matched to it. The silicide is ~15Å thick. The substrate and metal are initially separated by 1.8Å (determined by a quadric fit of the binding energy). The lateral dimensions are 11.5Å×11.5Å and 7.6Å×15.3Å in our (001)/(001) and (110)/(001) models, respectively. We apply 3.0%×-2.9% and 6.2%×-5.9% lateral strain to the metal layers to match them with the Si substrate and completely relax the ionic positions while keeping the lattice constants and simulation cell shape constant. After relaxation the residual stress is less than 0.6GPa in the (001)/(001) model and less than 1GPa in the (001)/(110) model.

We extract the p-type SBH from the calculated local electrostatic potential. Again, the potential is averaged over the x-y plane for each z value. A typical plot of the planar averaged local potential is shown in Fig. 5 b). Deep inside the Si and metal regions we expect to find bulk-like conditions in both materials. Within the bulk regions the planar averaged microscopic potential is also macroscopically averaged along the z-axis. The top of the valence band of Si in the bulk region is placed with respect to the averaged potential in the Si slab using a separate bulk calculation. The SBH is then easily extracted as shown in Fig. 5 b). Our results are summarized in Table 4. For our (001)/(001) model we find a SBH of 0.13eV for both PtSi and $Ti_xPt_{1-x}Si$. For our (110)/(001) model we find 0.11eV and 0.08eV for PtSi and $Ti_xPt_{1-x}Si$ contacts, respectively. The calculated barrier heights for PtSi contacts are in fair agreement with our previously reported value 0.16eV for the PtSi(001)/Si(001) interface [8], where a smaller cell (higher stress) was used to reduce the computational time. It is somewhat smaller than the experimental value of 0.2 eV [10].

Equation (1) suggests a linear increase in the SBH for decreasing WF. Although, in the previous section we found that Ti doping reduces the WF of PtSi by approximately 0.1eV

for the (001) and (110) Ti-terminated surfaces, our calculated barrier heights are rather insensitive to this change. To gain more insight we apply the metal induced gap states (MIGS) theory [20] for SBHs and compare with our results:

$$\varphi_p = E_g - S \cdot (\varphi_m - \varphi_{CNL}) - (\varphi_{CNL} - \chi). \quad (2)$$

Here E_g is the band gap of the semiconductor (1.1eV for Si), φ_m the metal WF, φ_{CNL} is the charge neutrality level (CNL) of the semiconductor, and χ its electron affinity. The pinning parameter S is believed to be an intrinsic property of the semiconductor surface. In the Schottky limit (S=1, *i.e.* no Fermi level pinning), equation (2) gives the "maximum dependence" on the WF. In the Bardeen limit (S=0, *i.e.* strong Fermi level pinning), the SBH does not depend on the metal WF at all. Equation (2) is a linear interpolation between the Schottky and Bardeen limits. In practice S, can be approximated by [21]:

$$S = \frac{1}{1 + 0.1 \cdot (\varepsilon_\infty - 1)^2}, \quad (3)$$

where ε_∞ is the high frequency limit of the dielectric constant of Si. Using ε_∞=11.7 the pinning parameter of Si is 0.08 indicating little dependence of the SBH on the WF. According to Bardeen, the CNL is the intrinsic property of the material and is essentially the Fermi level at the surface, in the literature theoretical values of the Si CNL vary between ~0.3eV and ~0.36eV above the valence band top, somewhat depending on the method of calculation [22,23,24]. For the CNL 0.3eV above the valence band top and electron affinity of 4.1 eV [25], in the Bardeen or strong pinning limit the SBH is always 0.30eV. In the Schottky limit the barrier height averaged over our (001)/(001) and (110)/(001) models is 0.13eV for PtSi/Si interfaces. For our $Ti_xPt_{1-x}Si$/Si interfaces it is 0.21eV, 0.08eV higher than for the PtSi/Si interfaces. This shift reflects the linear dependence of the SBH on the change in WF in the Schottky limit. However, our calculations indicate the difference between the SBH of $Ti_xPt_{1-x}Si$/Si and PtSi/Si interfaces of only 0.01eV suggesting little dependence of the SBH on the metal work function. Thus, our results are in qualitative agreement with the Bardeen model, *i.e.* the change in the WF does not influence the SBH, as is reflected by a small value of the pinning parameter S.

Impurity scattering in $Ti_xPt_{1-x}Si$ alloys

Thus far we have demonstrated that doping PtSi with Ti can increase the number of carriers without significantly altering the Schottky barrier to Si. However, doping typically is accompanied by the increase in scattering that may adversely affect the mobility. To analyze the change in the carrier mobility with increasing Ti concentration in bulk PtSi we use the Boltzmann transport formalism [26,27]. Assuming that collisions of electrons with substitutional Ti atoms are elastic and spin conserving, we can calculate the collision term in the Boltzmann equation, and estimate the change in the carrier

mobility of a system due to impurities. Similar calculations have been recently performed by Evans *et al.,* who analyzed the channel mobility degradation in a field effect transistor caused by interface defects [28].

To calculate the probability for an electron in band *n* with the wave vector $\vec{k}$ to scatter into band *m* with the wave vector $\vec{k}'$ we compute the impurity scattering potential ΔV and its scattering matrix element:

$$T_{mn}\left(\vec{k}',\vec{k}\right)=\left\langle n\vec{k}\left|\Delta V\right|m\vec{k}'\right\rangle, \tag{4}$$

where the unperturbed wave functions $\left|m\vec{k}'\right\rangle$ and $\left|n\vec{k}\right\rangle$ are the Bloch states of undoped PtSi normalized to unity, i.e. the absolute square of the wave function integrated over the primitive cell equals to one. The impurity scattering potential ΔV is calculated from first principles within density functional theory by subtracting the local potentials computed for a simulation cell of PtSi and $Ti_xPt_{1-x}Si$. Due to the metallic nature of PtSi the perturbation $|\Delta V|$ is short ranged and the integration in (4) can be reduced to an integral over the simulation cell provided it is sufficiently large. To ensure that the potential is fully contained in the simulation cell we calculate the carrier mobility in a 2×2×2 cell with one Ti impurity. In our approach we only relax the ionic positions in the perturbed and unperturbed cell, keeping the cell shape and volume fixed. The impurity potential is shown in fig. 8 in the form of crossectional contour plots in three orthogonal planes containing the impurity site. It ranges between -10eV and 10eV, and is roughly of the order of the kinetic energy of the fastest electron whose band velocity is 16 Å/fs (Fig. 9). The peak energy values of the potential are contained within a sphere of radius ~3Å around the Ti impurity, thus it is well contained in the simulation cell.

Using equation (4) and the Fermi golden rule we calculate the rate of scattering from state $\left|m\vec{k}'\right\rangle$ to state $\left|n\vec{k}\right\rangle$:

$$\Gamma_{mn}\left(\vec{k}',\vec{k}\right)=\tfrac{2\pi}{\hbar}\cdot n_d\cdot V\cdot\left|T_{mn}\left(\vec{k}',\vec{k}\right)\right|^2\delta\left(E_n\left(\vec{k}\right)-E_m\left(\vec{k}'\right)\right), \tag{5}$$

Where n_d is the impurity density, V is the volume of the simulation cell, and $E_n\left(\vec{k}\right)$ and $E_m\left(\vec{k}'\right)$ are the energy eigenvalues of the unperturbed wave functions $\left|n\vec{k}\right\rangle$ and $\left|m\vec{k}'\right\rangle$. The total rate is then obtained by summing over the first Brillouin zone multiplied by the probability for the initial state to be filled and the final state to be empty and subtracting the rates of backscattered carriers. The inverse scattering time for a state $\left|n\vec{k}\right\rangle$ is then given by:

$$\frac{1}{\tau_n\left(\vec{k}\right)} = \sum_{m,\vec{k}'} \Gamma_{mn}\left(\vec{k}', \vec{k}\right)\left(1 - \cos\left(\Theta_{\vec{k},\vec{k}'}\right)\right), \tag{6}$$

where the sum only runs over states within the range $-k_B T + E_F \le E \le E_F + k_B T$ as only these states contribute to scattering.

In equation (5) the δ-function ensures energy conservation. In practice we replace the δ-function by a properly normalized window function. Then scattering is only possible for states satisfying $\left|E_n\left(\vec{k}\right) - E_m\left(\vec{k}'\right)\right| < \varepsilon$. The width of the window function is 2ε. In our study we use the value ε=10meV (the difference to using ε=15meV in the later calculated mobility is within 5%). The carrier mobility is given by [27]:

$$\mu_{\alpha\beta} = -e\sum_{n,\vec{k}} \tau_n\left(\vec{k}\right)\left[\vec{v}_n\left(\vec{k}\right)\right]_\alpha \left[\vec{v}_n\left(\vec{k}\right)\right]_\beta \frac{\partial f_0\left(E_n\left(\vec{k}\right)\right)}{\partial E}. \tag{7}$$

In equation (7) the function $f_0\left(E_n\left(\vec{k}\right)\right)$ is the equilibrium Fermi-Dirac distribution with the chemical potential set to the Fermi energy of the system. The band velocity $\vec{v}_n$ is the derivative of the energy $E_n\left(\vec{k}\right)$ with respect to $\vec{k}$ divided by $\hbar$. Figure 9 shows the probability density distribution of the band velocity within $\pm k_B T$ of the Fermi level. We calculate velocity magnitudes and normalize the sum to one. The distribution peaks at 2Å/fs. The sum in (7) runs over ten contributing bands at the Fermi level. Using equation (7) the conductivity is given by

$$\sigma_{\alpha\beta} = en\mu_{\alpha\beta}. \tag{8}$$

For the electron density n in equation (8) we use our previously estimated conduction electron density within the energy interval $-k_B T + E_F \le E \le E_F + k_B T$ (Table 1).

We calculate the mobility and conductivity tensors of $Ti_xPt_{1-x}Si$ alloys for several Ti concentrations. Our calculations show that dense k-point meshes are crucial for accurate convergence of the conductivity tensor. We use a 10×10×12 mesh for the 2×2×2 simulation cell. Our results are listed in Table 5. It is important to note that in this theory no electron-phonon or any other types of interactions besides the impurity scattering are included. Thus, the result is not the absolute value for the carrier mobility but rather a correction to the unperturbed absolute values. The total mobility and conductivity are calculated using the following expressions:

$$\frac{1}{\mu_{tot}} = \frac{1}{\mu_0} + \frac{1}{\mu_d} \rightarrow \mu_{tot} = \frac{\mu_d}{1+\mu_d/\mu_0}$$

$$\sigma_{tot} = en\mu_{tot} . \qquad (9)$$

The subscript "d" denotes the defect contribution calculated in this work whereas "0" denotes the absolute values without impurity scattering for which we use the experimental value. We use $\sigma_0 \approx 3.3 \cdot 10^6$A/Vm [29] and $\mu_0 = \sigma_0/en_0 \approx 263.5\text{cm}^2/\text{Vs}$.

In Figure 10 we plot μ_{tot} and σ_{tot}. For μ_d and σ_d we use the average of the principle values of our calculated tensors. The mobility and conductivity tensors for 1.56%, 3.13%, 6.25% and 12.5% Ti are listed in Table 5. Clearly the carrier mobility decreases with the increasing number of impurities. Contrary to what happens in doped semiconductors, the carrier density rises too slowly to offset the decrease in mobility, and conductivity decreases. However, for Ti concentrations below 0.5% the decrease in conductivity is less than 50% compared to bulk PtSi.

Thermodynamic stability and solubility limit

The question now arises whether one can incorporate the sufficient amount of Ti on the Pt site in PtSi. Multi-component silicides can be produced by depositing layers of metals on a Si substrate and subsequent heating until silicidation sets in. Typically, four reaction outcomes are distinguished: layer reversal, phase separation, solid solution or ternary compound formation. These reactions can occur successively, for further details we refer the interested reader to the work by Setton *et. al.* [30]. Since both Ti and Pt form silicide phases, one could in principle, encounter formation of Ti_nSi, Pt_nSi, $PtTi_n$, their mixtures or a ternary compound. To simplest approximation the alloy with the lowest formation energy would form first, followed by the alloy with the next highest formation energy, and so on. We calculate the heat of formation of PtTi, PtSi and TiSi to be ΔH_{PtTi} = −1.72eV, ΔH_{PtSi} = −1.43eV and ΔH_{TiSi} = −1.72eV per formula unit, respectively. Considering just these three compounds (not including higher order silicides and titanides) the heats of formation indicate that upon heating the Ti/Pt/Si system, PtTi or TiSi would form first. $TiPt_n$ alloys are indeed well known experimentally [31, 32]. The formation of PtSi, $Ti_xPt_ySi_z$ or $Ti_xPt_{1-x}Si$ compounds would occur at higher temperature.

The formation energy per formula unit of PtSi is higher than that of TiSi, suggesting that the substitution of Pt by Ti in PtSi would result in a stable $Ti_xPt_{1-x}Si$ alloy. By analyzing the changes in the internal energy after alloying we identify the energetically preferred substitution site. The formation energy can be estimated by

$$PtSi + xTi \xrightarrow{\Delta E} Ti_x Pt_{1-x} Si + xPt\,, \tag{10}$$

and

$$PtSi + xTi \xrightarrow{\Delta E} Ti_x PtSi_{1-x} + xSi \tag{11}$$

for doping on the Pt and Si-site, respectively. The reaction energy in (10) and (11) and the cell volume V of the alloys are plotted in Figure 11 as function of Ti concentration. The cell volume V will be used later. Doping on a Pt-site we find a stable alloy with approximately 0.5% Ti. Above 0.5% the formation energy increases linearly with the Ti concentration. Doping on a Si-site becomes energetically favorable over doping on a Pt-site for more than ~1.8% Ti. We find a linear increase in the cell volume when doping on a Si-site. However, mixing up to 2% Ti on a Pt-site "shrinks" the cell. Above 2% its volume starts increasing linearly. Interestingly, Ti's atomic radius is 5% larger than that of Pt yet producing a net volume decrease in the cell size compared to PtSi.

To estimate Ti's solubility limit in PtSi, we calculate the change in free energy after alloying:

$$\Delta G = \Delta E + p\Delta V - TS_m\,. \tag{12}$$

Here ΔE is the change in internal energy, $p\Delta V$ is the contribution due to the change in volume and TS_m accounts for the change in entropy. For ΔE we use the values calculated using reactions (10) and (11). The $p\Delta V$ term is calculated from the change in the volume after alloying multiplied by p=1atm. The entropic contribution in (12) is estimated using a simple theory of ideal binary mixtures:

$$S_m = -k_B \ln\left(\frac{N_1!\times N_2!}{N_{total}!}\right). \tag{13}$$

Assuming Ti is substituted either for Pt or Si, N_1 is the number of Ti atoms, $N_2 = N_{Pt/Si} - N_1$ the number of remaining Pt or Si atoms, and $N_{tot} = N_1 + N_2$. The entropic term is stabilizing the alloys above the "critical temperature" when ΔG becomes negative. The critical temperature is determined by the condition ΔG=0 in (12):

$$T_{crit} = \frac{\Delta E + p\Delta V}{S_m}, \qquad (14)$$

where the ΔE, $p\Delta V$ and S_m terms depend on the Ti-concentration. Therefore, plotting equation (14) as a function of the Ti-concentration shows the solubility limit of Ti in PtSi at a particular critical temperature.

Our results for T_{crit} are summarized in Table 1 and Figure 12. Up to approximately 0.7% Ti mixes on the Pt-site. Above ~0.7% the solubility limit of Ti increases linearly with temperature. At 500K up to ~0.9% Ti can be mixed in PtSi (substituting Pt), while at PtSi's congruential melting temperature 1500K only up to ~2% Ti can be mixed on the Pt-site. This can be traced to a chemical difference manifested in the Pt-Si and Ti-Si bond lengths. We find that the nearest neighbor distance in TiSi is 2.6Å, while in PtSi it is 2.4 Å, deviating by 7.5% from each other. Thus, alloying introduces significant local stress. On the other hand up to ~3% Ti can be mixed on the Si-site at 500K. We have also considered a possibility of Ti clustering, and find that it is not energetically preferable. To obtain a notable gain in the carrier density with increasing Ti concentration, 1.8% and more Ti should mix on the Pt-site. Thus, in section IV we analyze possible routes to increase the Ti solubility limit at low temperature and to stabilize $Ti_xPt_{1-x}Si$ *vs.* Ti_xPtSi_{1-x} alloys.

IV. Co-doping with boron, carbon, gallium and aluminum

One can think of several ways to increase the solubility of Ti in PtSi. The parameters in equation (14) controlling the solubility limit are the formation energy ΔE, the cell volume and the entropy of mixing. The solubility limit increases when either ΔE or the cell volume decrease, the entropy of mixing increases, or if any combination of these three possibilities occurs. Our smallest 2×2×2 cell for 1.56% Ti is 2.3Å^3 smaller than bulk PtSi. Our largest 2×2×2 cell for 3.13% Ti is 6.6Å^3 larger than PtSi. Assuming pressure of 1 atm the $p\Delta V$ term in (14) ranges between $-1.4\cdot10^{-3}$meV and $4.1\cdot10^{-3}$meV, less than 0.07% of the smallest energy difference we calculate using (10) and (11). Thus, the $p\Delta V$ contribution is too small on the scale of ΔE to make a significant difference in alloy's stability (equation 14). Instead, we consider co-doping TiPtSi with boron, carbon, gallium and aluminum ions (later denoted as "X") to increase the entropic contribution and hopefully reduce ΔE. We use alloys with 3.13% and 6.25% concentration of Ti. Here, we at first only consider doping Ti on the Pt-site while co-doping with one of the proposed elements. For the energetically preferred co-dopant we later re-evaluate the preferred doping site of Ti.

We use a 2×2×2 simulation cell and substitute one X atom on either the Pt or the Si-site. Despite the large difference in the atomic radii of our co-dopants and Pt and Si we find

that all of the proposed co-dopants prefer to mix substitutionally on the Si-site. The formation energy of the $Ti_xPt_{1-x}X_ySi_{1-y}$ is estimated using the following reactions:

$$32PtSi + 2Ti + X \xrightarrow{\Delta E} Ti_2Pt_{30}XSi_{31} + 2Pt + Si\,, \tag{15}$$

and

$$32PtSi + 4Ti + X \xrightarrow{\Delta E} Ti_4Pt_{28}XSi_{31} + 4Pt + Si \tag{16}$$

for 3.13% and 6.25% Ti, respectively. The formation energy for all co-dopants along with the carrier density at the Fermi level are summarized in Table 6. In all alloys the carrier density at the Fermi level is increased compared to bulk PtSi. While co-doping with boron and carbon increases the formation energy of the alloy, gallium or aluminum lower the formation energy drastically. We find the largest decrease in formation energy when using Al as co-dopant and identify a marginally stable $Ti_xPt_{1-x}Al_ySi_{1-y}$ alloy with 3.12% Ti.

For this alloy we also consider introducing Ti on a Si-site to identify the preferences of the mixing site. The formation energy is calculated from

$$32PtSi + 2Ti + Al \xrightarrow{\Delta E} Ti_2AlPt_{32}Si_{29} + 3Si\,. \tag{17}$$

It is -10meV/atom or 6.5meV/atom smaller than when mixing Ti on the Pt-site. The energy difference is very small, suggesting that Ti will occupy both the Pt and the Si sites with equal probability. Thus, independent on which site Ti mixes the alloy's stability can be increased through co-doping with Al.

Using the formation energy calculated in (15) and (16) in equation (14) we recalculate the solubility limit of titanium. For the entropic contribution we assume that Ti only mixes on the Pt-site while the co-dopant X only mixes on the Si-site. The entropy of mixing is then 1.3×10^{-5}eV/K and 1.2×10^{-5}eV/K in $Ti_2Pt_{30}XSi_{31}$ (3.13% Ti) and $Ti_4Pt_{28}XSi_{31}$ (6.25% Ti), respectively. The critical temperatures are summarized in Table 6, the solubility limit of Ti is shown in Figure 12. While B and C don't improve the solubility, Ga and Al increase it significantly when compared to both $Ti_xPt_{1-x}Si$ and Ti_xPtSi_{1-x}. At room temperature more than 4% Ti can be mixed in PtSi when co-doping with Al. A linear interpolation between $Ti_2Pt_{30}AlSi_{31}$ and $Ti_4Pt_{28}AlSi_{31}$ suggests a 1.5-fold increase in carrier density for 4% Ti compared to bulk PtSi.

So far we have only considered reactions between PtSi and other elements. To analyze the possible alloy decomposition we consider reactions competing with the formation of $Ti_xPt_{1-x}X_ySi_{1-y}$. In order to do so, we calculate the reaction energy of two reactions:

$$Ti_2Pt_{30}XSi_{31} \xrightarrow{\Delta E} 30PtSi + TiSi + TiX \,, \tag{18}$$

and

$$Ti_4Pt_{28}XSi_{31} \xrightarrow{\Delta E} 28PtSi + 3TiSi + TiX \,, \tag{19}$$

for 3.12% and 6.25% Ti, respectively. The energies for the PtSi, TiSi and TiX are extracted from the respective bulk calculations. To keep the analysis simple, we do not consider reactions with higher order silicides such as $PtSi_2$ or $TiSi_2$. Negative reaction energy indicates thermodynamically preferred decomposition. We find negative energy in all cases except when co-doping a 3.13% alloy with aluminum. In this case, the reaction energy is 8.2meV/atom. Unlike other alloys, this one does not have a thermodynamic preference to decompose into a mixture of binary intermetallics PtSi, TiSi and TiAl.

V. Conclusions

We use theoretical band engineering to analyze and find ways to control the electrical properties of technologically important contact material PtSi. We find that alloying PtSi with Ti may considerably increase the number of carriers. The improvement comes from the introduction of titanium d-states near the Fermi level. Moreover, we find that though doping with Ti lowers the work function of PtSi by as much as 0.45eV, the Schottky barrier height to Si is rather insensitive to this change. Using a combination of density functional theory and Boltzmann transport formalism we show that the increase in carrier concentration is accompanied by alloy scattering that adversely affects conductivity despite a significant increase in the number of carriers. In particular, for the doping concentration of 2% we find a 60% decrease in conductivity as compared to bulk PtSi. The thermodynamic analysis indicates that under equilibrium conditions at room temperature only 0.7% Ti can be mixed in PtSi substituting Pt. The low solubility is attributed to strain caused by Ti in the PtSi lattice. To achieve higher doping concentrations we suggest co-doping PtSi with gallium or aluminum. While aluminum is best, both increase Ti solubility at room temperature to more than 3%.

Acknowledgement

We wish to thank Conal Murray of IBM research for stimulating discussions. This work was supported by the National Science Foundation under Grant DMR1006725, and Texas Advanced Computing Center.

References

1. S. Yhang, M. Ostling, CRC Crit. Rev. Solid State Mater. Sci. **28**, 1 (2003).

2. C. Detavernier, A. S. Ozcan, J. Jordan-Sweet, E. A. Stach, J. Tersoff, F. M. Ross, C. Lavoie, Nature (London) **426**, 641 (2003).

3. Detavernier, C. Lavoie, Appl. Phys. Lett. **84**, 3549 (2004).

4. E. H. Rhoderick and R. H. Williams, *Metal-Semiconductor Contacts (Electrical & Electronic Engineering Monographs)*, 2nd edition, Oxford Univ. Press, 1988.

5. J. E. Klepeis, O. Beckstein, O. Pankratov, G. L. W. Hart, Phys. Rev. B **64**, 155110 (2001).

6. N. Franco, J. E. Klepeis, C. Bostedt, T. Van Buuren, C. Heske, O. Pankratov, T. A. Callcott, D. L. Ederer, L. J. Terminello. Phys. Rev. B **68**, 045116 (2003).

7. O. Beckstein, J. E. Klepeis, G. L. W. Hart, and O. Pankratov. Phys. Rev. B **63**, 134112 (2001).

8. M. K. Niranjan, S. Zollner, L. Kleinman, A. A. Demkov. Phys. Rev. B **73**, 195332 (2006).

9. H. Bentmann, A. A. Demkov, R. Gregory, S. Zollner. Phys. Rev. B **78**, 205302 (2008).

10. V. W. Chin, M. A. Green, J. W. V. Storey, Solid-State Electron. **36**, 1107 (1993).

11. E. J. Graeber, R. J. Baughman and B. Morossin, Acta Crystallogr. **29**, 1991 (1973).

12. D. Vanderbilt, Phys. Rev. B **41**, 7892 (1990).

13. G. Kresse, J. Hafner, Phys. Rev. B **47**, 558 (1993).

14. G. Kresse, J. Furthmüller, Comput. Mat. Sci. **6**, 15 (1996).

15. G. Kresse, J. Furthmüller, Phys. Rev. B **54**, 11169 (1996).

16. G. Kresse, J. Hafner, J. Phys: Condens. Matt. **6**, 8245 (1994).

17. G. Kresse, D. Joubert, Phys. Rev. B **59**, 1758 (1999).

18. H. J. Monkhorst and J. D. Pack, Phys. Rev. B **13**, 5188 (1976).

19. W. A. Harrison, *Elementary Electronic Structure (Revised Edition)*, World Scientific Publishing, 2004.

20. V. Heine, Phys. Rev. **138**, A1689 (1965).

21. W. Mönch, *Electronic structure of metal-semiconductor contacts* (Kluwer, Dordrecht, 1990).

22. J. Robertson and B. Falabretti, J. Appl. Phys. **100**, 014111 (2006).

23. J. Tersoff, Phys. Rev. B **30**, 4874 (1984).

24. M. Elices and F. Yndurain, J. Phys. C: Solid State Phys. **5**, L146 (1972).

25. S. M. Sze, *Physics of semicondurtor devices*, Wiley, New York (1981).

26. H. Bruus, K. Flensburg, "Many-Body Quantum Theory in Condensed Matter Physics: An Introduction", Oxford University Press (2004).

27. G. Mahan, "Many-Particle Physics", 2nd edition, Plenum New York 1990).

28. M. H. Evans, X.-G. Zhang, J. D. Joannopoulos, S. T. Pantelides, Phys. Rev. Lett. **95**, 106802 (2005).

29. P. I. Gaiduk and A. Nylandsted Larsen, Appl. Phys. A **53**, 167 (1991).

30. M. Setton, J. van der Spiegel, Thin Sol. Films **156**, 351 (1988).

31. L. S. Hung, J. W. Mayer, J. Appl. Phy. **60**, 1002 (1986).

32. T. Biggs, L. A. Cornish, M. J. Witcomb, M. B. Cortie, J. All. Comp. **375**, 120 (2004).

31_R. R. E. Smallman, W. Hume-Rothery, C. W. Haworth, *The structure of metals and alloy*, The Institute of Metals, *5th edition* (1988).

32_R. Hung, Q. Z. Hong, J. W. Mayer, J. Appl. Phys. **63**, 1749 (1988).

Table 1. DOS at the Fermi level and carrier density in $Ti_xPt_{1-x}Si$ and Ti_xPtSi_{1-x} alloys for different Ti concentration. The DOS is given per 2×2×2 cell. For Ti concentration higher than 1% we observe an increase in both the DOS and carrier density for doping on either site.

at. %Ti	Ti on Pt-site			Ti on Si-site		
	DOS at E_F [*el./e*V×V_{Cell}]	*n* [10^{20} el./cm^3]	T_{crit} [K]	DOS at E_F [*el./e*V×V_{Cell}]	*n* [10^{20} el./cm^3]	T_{crit} [K]
0.00	14.5	7.9	0	14.5	7.9	0
0.52	14.9	7.7	0	13.2	6.6	1814
1.04	15.1	8.6	879	16.6	9.2	1508
1.56	15.9	9.1	905	14.8	8.6	1337
3.13	18.0	9.4	1532	13.5	7.6	618
6.25	17.0	13.8	2809	---	---	---
12.50	25.2	21.5	3618	---	---	---

Table 2. Experimental and theoretical internal in plane coordinates in orthorhombic Pnma cell of PtSi. Pt atoms are located at [$u_{Pt,}$ v_{Pt}, 1/4], [1/2-$u_{Pt,}$ v_{Pt}-1/2, 1/4], [1-$u_{Pt,}$ 1-v_{Pt}, 3/4], [1/2+$u_{Pt,}$ 3/2-v_{Pt}, 3/4] whereas Si atoms are located at [$u_{Si,}$ v_{Si}, 1/4], [3/2- $u_{Si,}$ 1/2+v_{Si}, 1/4], [u_{Si}-1/2, 1/2- v_{Si}, 3/4], [1- $u_{Si,}$ 1- v_{Si}, 3/4]. The positions are given in fractional coordinates.

	u_{Pt}	v_{Pt}	u_{Si}	v_{Si}	Ref.
Exp.	0.1922	0.9956	0.583	0.177	11
Theory	0.1920	0.9980	0.585	0.178	This work

Table 3. Theoretical work functions for $Ti_xPt_{1-x}Si$ with 3.13 at.% Ti and bulk PtSi. Ti-terminated surfaces have lower work function compared to the corresponding PtSi surfaces with the exception of the (101) orientation.

(hkl)	**termination**	**φ [eV]**	
		$Ti_xPt_{1-x}Si$	**PtSi**
001	st.	5.28	5.22
	Ti	5.14	---
010	Pt	5.40	5.39
	Si	5.10	5.24
	Ti	4.94	---
100	Pt	5.11	5.11
	Si	5.02	5.02
	Ti	4.73	---
101	Si	5.15	5.03
	Ti	5.25	---
011	Pt	5.23	5.18
	Si	5.26	5.12
	Ti	5.00	---
110	Pt	5.06	4.96
	Si	5.35	5.29
	Ti	4.88	---

Table 4. Comparison of the SBHs extracted from local potential plots with the MIGS theory, and Bardeen and Schottky models. The Ti concentration in the $Ti_xPt_{1-x}Si$ alloys is 3.13 at.%.

[a] US pseudopotentials [8]

interface (metal/Si)	VASP SBH [eV]		MIGS SBH [eV]		BL [eV]		SL [eV]	
	PtSi	TiPtSi	PtSi	TiPtSi	PtSi	TiPtSi	PtSi	TiPtSi
001/001	0.13	0.13	0.28	0.28			0.00	0.08
110/001	0.11	0.08	0.30	0.30	0.30		0.26	0.34
001/001[a]	0.16	---	0.29	---			---	---

Table 5: Carrier mobility and conductivity tensors of $Ti_xPt_{1-x}Si$ due to impurity scattering. The considered Ti concentrations are 1.56 at.%, 3.13 at.%, 6.25 at.% and 12.5 at.%. For comparison, the isotropic conductivity of silver is ~$63 \cdot 10^6$ A/Vm.

at. %Ti	μ_d (cm^2/Vs)	PV (cm^2/Vs)	σ_d (10^6 A/Vm)	PV's (10^6 A/Vm)
12.5	$\begin{pmatrix} 12.0 & -0.6 & 1.9 \\ -0.6 & 10.2 & -0.9 \\ 1.9 & -0.9 & 14.3 \end{pmatrix}$	$\begin{pmatrix} 10.0 \\ 10.9 \\ 15.6 \end{pmatrix}$	$\begin{pmatrix} 0.41 & -0.02 & 0.07 \\ -0.02 & 0.35 & -0.03 \\ 0.07 & -0.03 & 0.49 \end{pmatrix}$	$\begin{pmatrix} 0.34 \\ 0.37 \\ 0.53 \end{pmatrix}$
6.25	$\begin{pmatrix} 24.0 & -1.1 & 3.9 \\ -1.1 & 20.5 & -1.8 \\ 3.9 & -1.8 & 28.6 \end{pmatrix}$	$\begin{pmatrix} 20.1 \\ 21.8 \\ 31.2 \end{pmatrix}$	$\begin{pmatrix} 0.53 & -0.02 & 0.09 \\ -0.02 & 0.45 & -0.04 \\ 0.09 & -0.04 & 0.63 \end{pmatrix}$	$\begin{pmatrix} 0.44 \\ 0.48 \\ 0.69 \end{pmatrix}$
3.13	$\begin{pmatrix} 47.9 & -2.2 & 7.7 \\ -2.2 & 41.0 & -3.6 \\ 7.7 & -3.6 & 57.1 \end{pmatrix}$	$\begin{pmatrix} 40.1 \\ 43.5 \\ 62.4 \end{pmatrix}$	$\begin{pmatrix} 0.72 & -0.03 & 0.12 \\ -0.03 & 0.62 & -0.05 \\ 0.12 & -0.05 & 0.86 \end{pmatrix}$	$\begin{pmatrix} 0.60 \\ 0.66 \\ 0.94 \end{pmatrix}$
1.56	$\begin{pmatrix} 95.8 & -4.5 & 15.4 \\ -4.5 & 81.9 & -7.3 \\ 15.4 & -7.3 & 114.3 \end{pmatrix}$	$\begin{pmatrix} 80.2 \\ 87.1 \\ 124.7 \end{pmatrix}$	$\begin{pmatrix} 1.40 & -0.07 & 0.22 \\ -0.07 & 1.19 & -0.11 \\ 0.22 & -0.11 & 1.67 \end{pmatrix}$	$\begin{pmatrix} 1.17 \\ 1.27 \\ 1.82 \end{pmatrix}$

Table 6. Reaction energy, carrier concentration and critical temperature of $Ti_2Pt_{30}XSi_{31}$ (3.13 at.% Ti) and $Ti_4Pt_{28}XSi_{31}$ (6.25 at.% Ti) alloys. Negative critical temperature indicates stable alloys as the numerator in equation (14) becomes negative. Co-doping with Ga and Al yields a large increase in the solubility limit at a given temperature compared to pure $Ti_xPt_{1-x}Si$ alloys.

X	**3.13 at.% Ti**			**6.25 at.% Ti**		
	***ΔE* [eV/atom]**	***T*$_{crit}$ [K]**	***n* [10^{20} cm^{-3}]**	***ΔE* [eV/atom]**	***T*$_{crit}$ [K]**	***n* [10^{20} cm^{-3}]**
---	0.013	1532	9.4	0.021	2809	13.8
B	0.029	2211	10.0	0.042	3477	11.1
C	0.051	3933	8.3	0.063	5168	15.1
Ga	0.003	269	10.9	0.018	1474	11.9
Al	-0.004	0	11.3	0.012	983	12.7

Figure 1: DOS of bulk PtSi in a 2×2×2 supercell. The zero of energy is set to the Fermi level. The arrow indicates how the Fermi level has to be moved to a hypothetical energy (dashed line) in order to provide a large carrier concentration accessible for electrical conductivity.

Figure 2:
a) Primitive cell of bulk PtSi. PtSi crystallizes in the primitive orthorhombic structure with a MnP-type lattice with space group Pnma (*#62 in the International X-Ray Tables*). The lattice constants are: a = 5.922 Å, b = 5.575 Å, c = 3.586 Å [11]. The smaller balls are Pt, and the bigger balls are Si atoms. The exact positions of all atoms are summarized in Table 2.

b) Primitive cell of bulk TiSi. TiSi crystallizes in the primitive orthorhombic structure with a FeB-type lattice with space group Pnma. The lattice constants are a = 6.544 Å, b = 4.997 Å, c = 3.638 Å.

Figure 3: Top to bottom: DOS of bulk PtSi, $TiPt_{31}Si_{32}$, $Ti_2Pt_{30}Si_{32}$, $Ti_4Pt_{28}Si_{32}$, $Ti_8Pt_{24}Si_{32}$ corresponding to 0%, 1.56 at.%, 3.13 at.%, 6.25 at.% and 12.5 at.% Ti. E_F is at 0. The DOS is calcualted with respect to a 2×2×2 cell of bulk PtSi.

Figure 4: Total DOS and d-states of bulk PtSi (top) and $Ti_8Pt_{24}Si_{32}$ (12.5 at.% Ti, bottom). The zero of energy is set to the Fermi level. The Ti d-states appear right at the Fermi level thus increasing the carrier concentration considerably compared to PtSi.

Figure 5: a) Local potential and planar averaged local potential of (100) $Ti_xPt_{1-x}Si$ surface. The difference in energy between the vacuum level and the highest occupied level in the metal (*i.e.* the Fermi level) is the work function of the calculated surface.
b) Local potential and planar averaged potential of a (001)/(110) $Ti_xPt_{1-x}Si$/Si interface. Indicated are also the top of the valence band and the bottom of the conduction band of Si bulk. The difference between the top of the valence band and the Fermi level of the system is the p-type SBH.

Figure 6: Surface models with Si termination (Si on top of the surface), Pt termination and a termination with Ti atoms at the surface. All surfaces shown are (100) oriented."

Figure 7: Calculated work functions of PtSi (diamonds) and $Ti_xPt_{1-x}Si$ alloys (squares). Except for the (101) orientation the work function of $Ti_xPt_{1-x}Si$ decreases by up to ~0.5eV compared to PtSi.

Figure 8: Contour plots of the scattering potential of a Ti impurity in a 2×2×2 cell of bulk PtSi. The Ti is placed substitutionally on a Pt-site. The position of the impurity is indicated by the cross. The impurity potential varies from -15eV to 15eV.

Figure 9: Distribution of band velocities within $\pm k_B T$ at room temperature around the Fermi level. The highest calculated velocity is 16Å/fs. The distribution peaks at 2Å/fs.

Figure 10: μ_{tot} and σ_{tot} for $\mu_0 \approx 263.5 cm^2/Vs$ and $\sigma_0 = \frac{1}{\rho_0} \approx 3.3\times10^6 A/Vm$ (from ref. 27). μ_0 is obtained by dividing σ_0 by the elementary charge and carrier density. We find a monotonic degradation of conductivity for higher Ti-concentration.

Figure 11: Formation energy and cell volume of the $Ti_xPt_{1-x}Si$ and Ti_xPtSi_{1-x} alloys. For low Ti concentrations (<1.8 at.%) titanium prefers to be mixed on the Pt-site. Above this concentration it tends to mix on the Si-site.

Figure 12: Solubility limit of Ti in different alloy compositions with and without co-doping. While the x-fraction of Ti in the alloy is variable, the y-fraction (co-dopants) is fixed to 1/32 (corresponding to 1.56 at.%). The best co-dopant is Al yielding stable alloys with up to 4 at.% Ti.

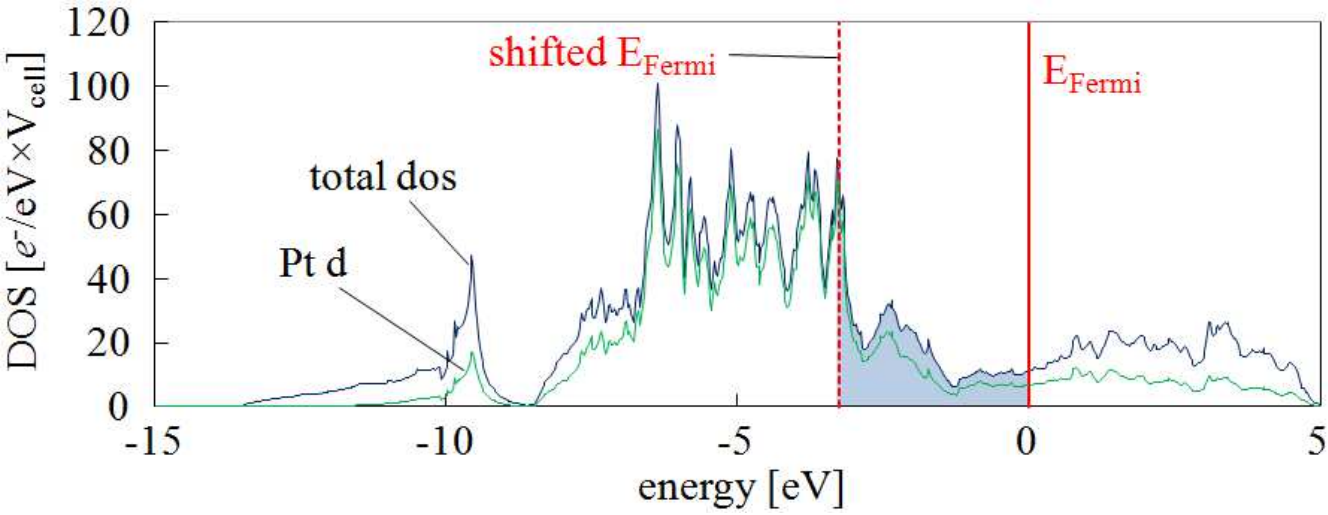

Figure 1 BF11678 19DEC2011

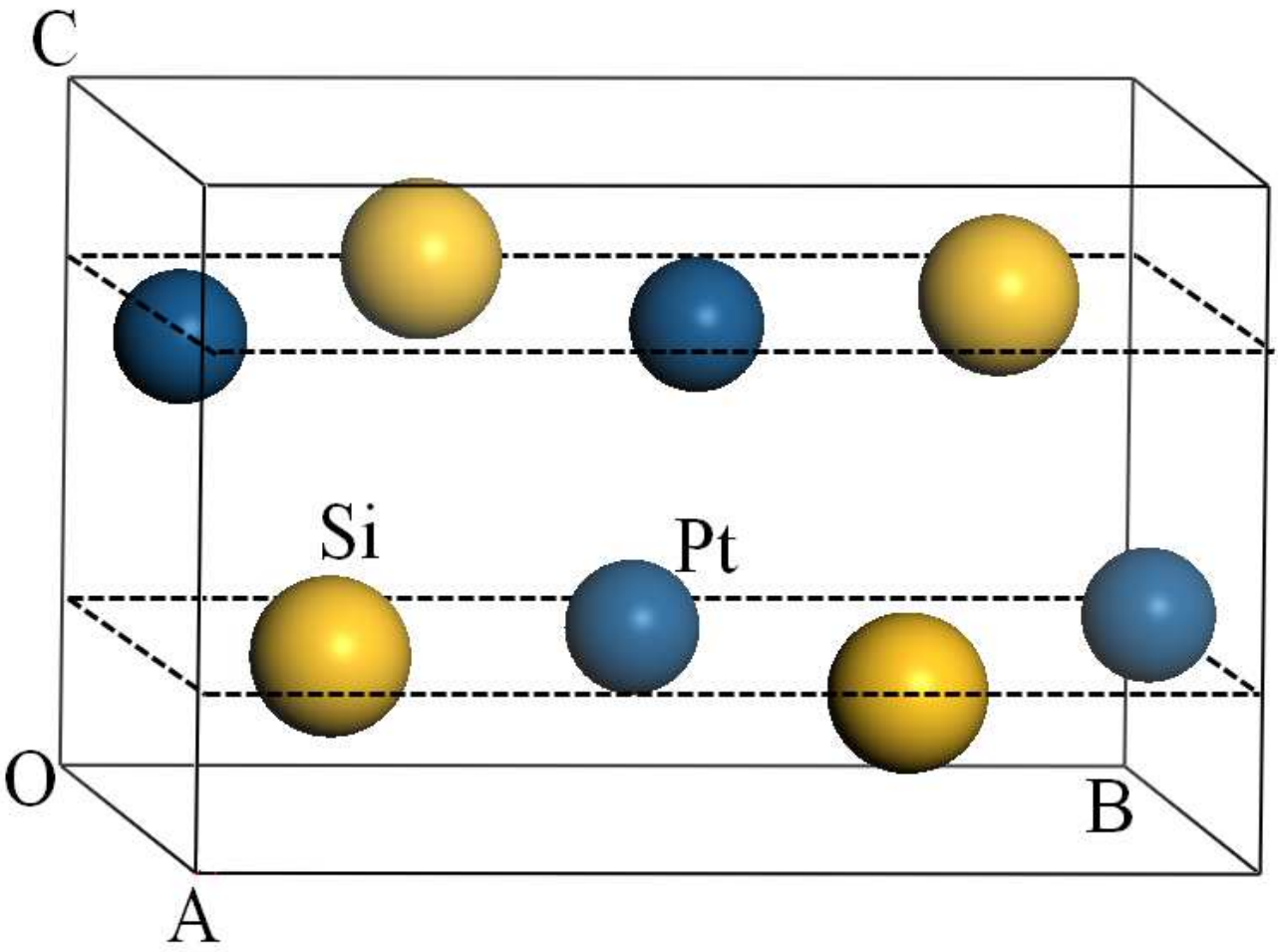

Figure 2a BF11678 19DEC2011

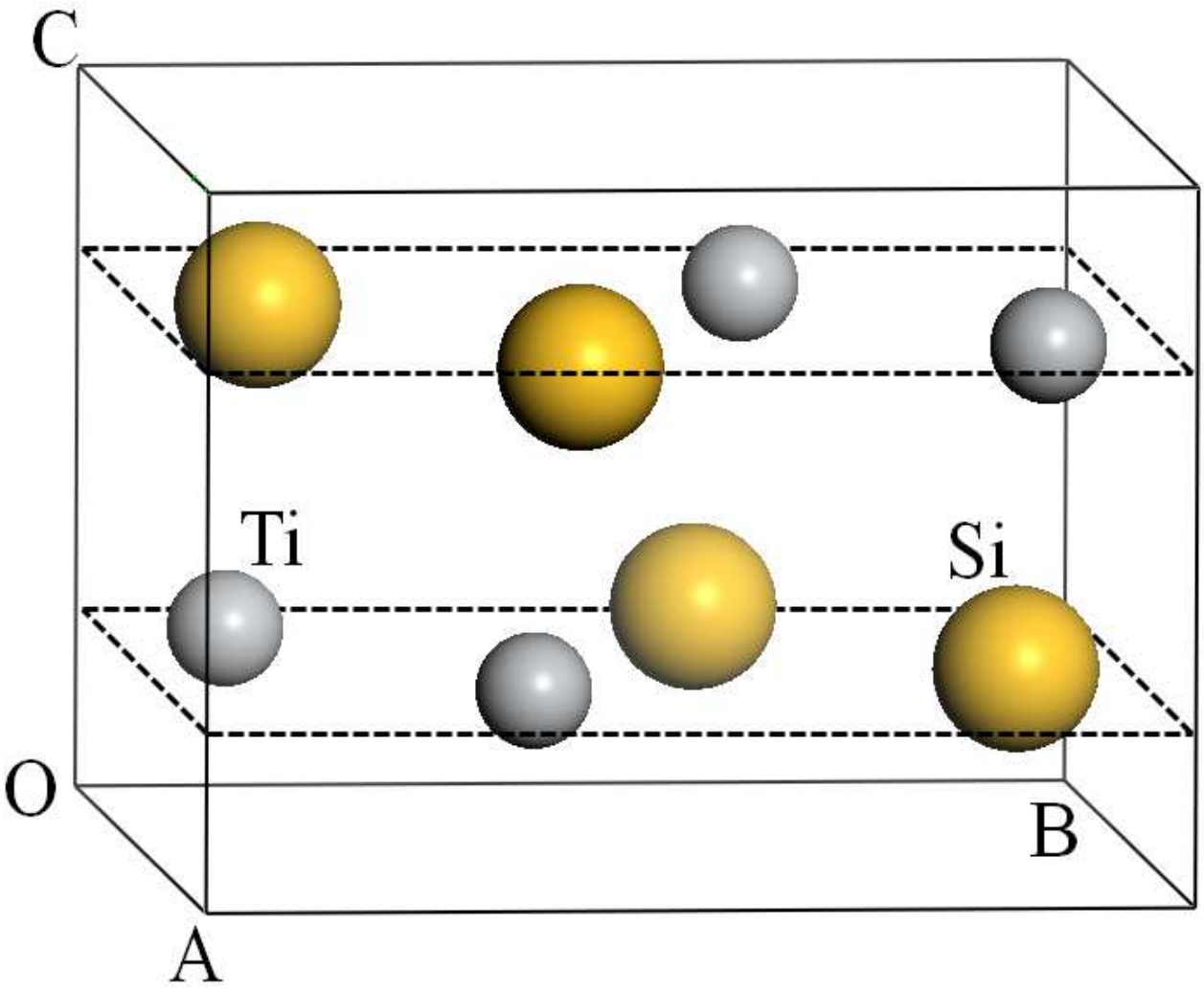

Figure 2b BF11678 19DEC2011

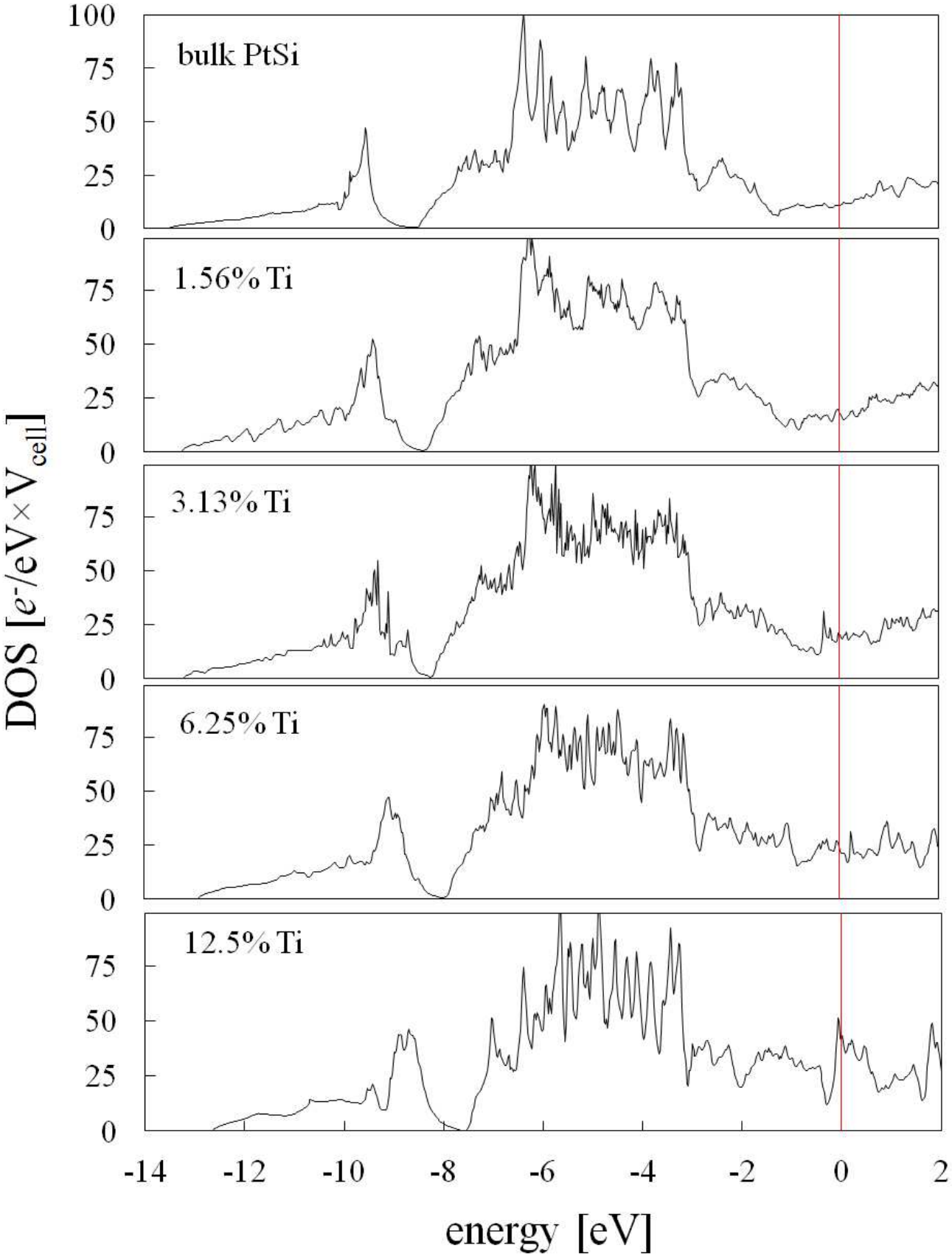

Figure 3 BF11678 19DEC2011

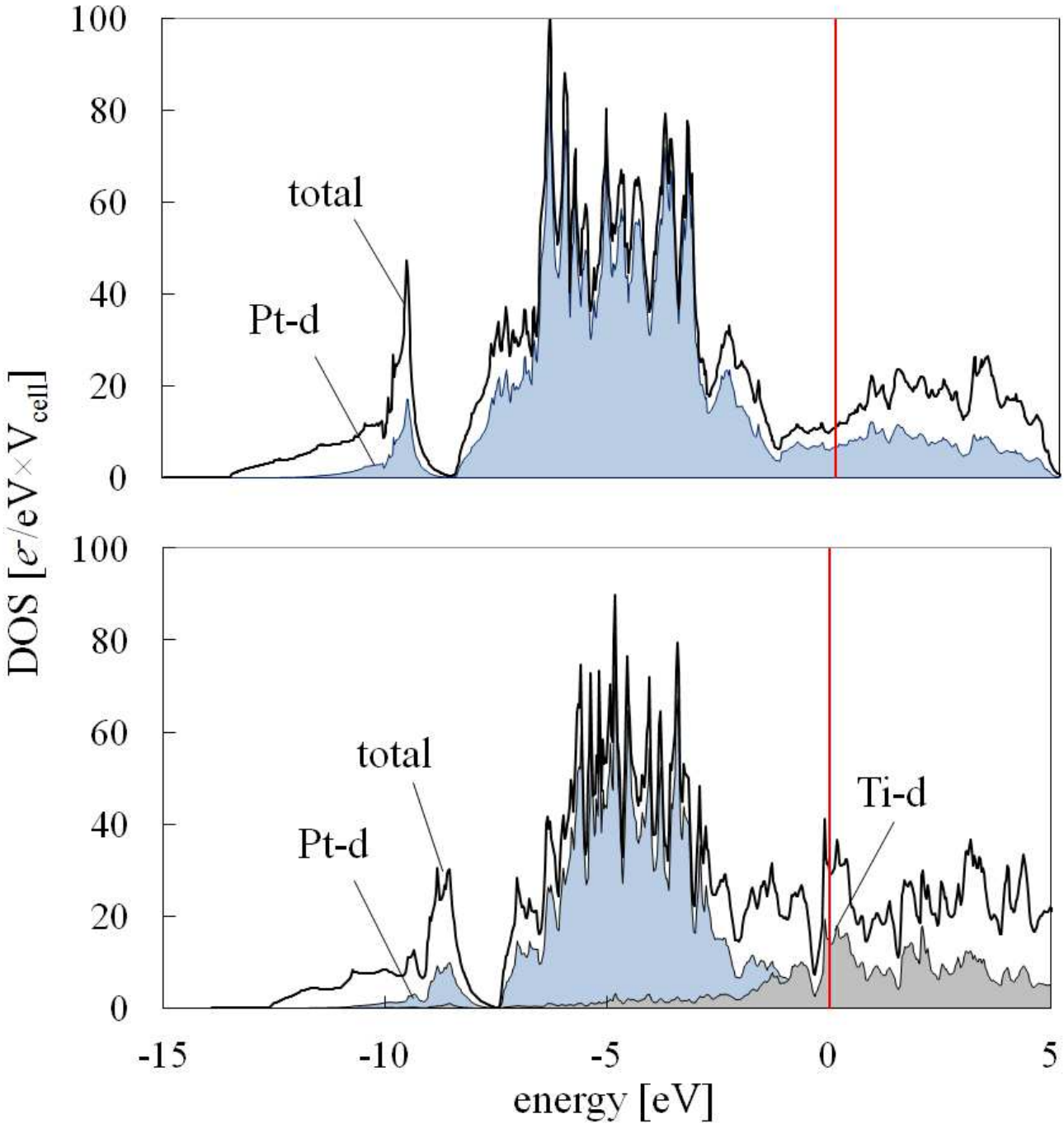

Figure 4 BF11678 19DEC2011

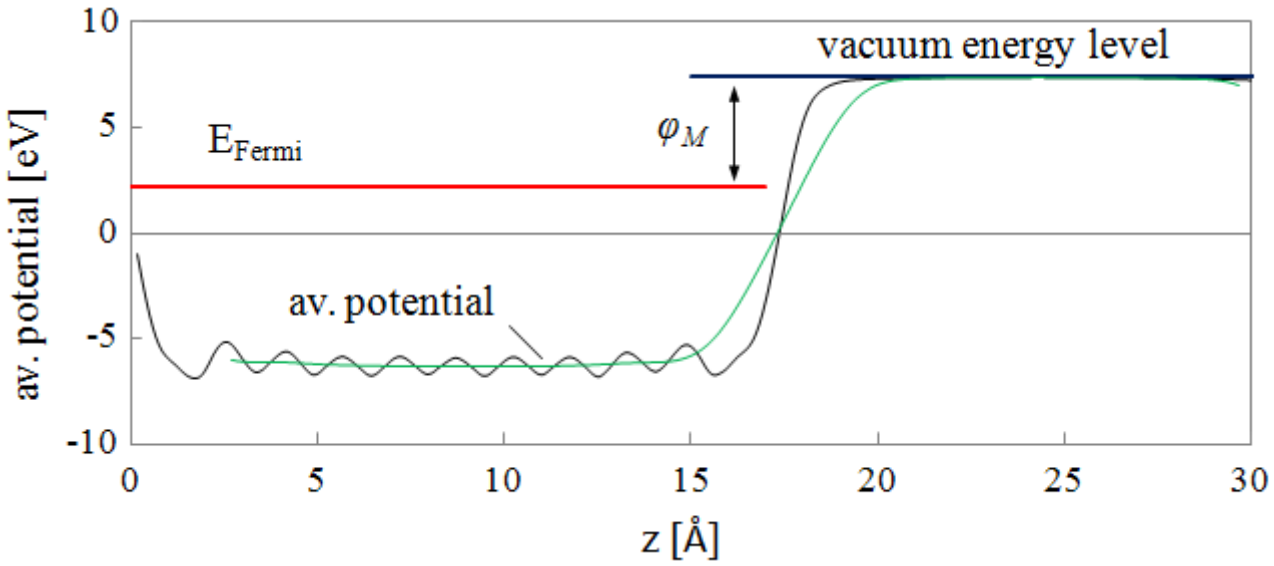

Figure 5a BF11678 19DEC2011

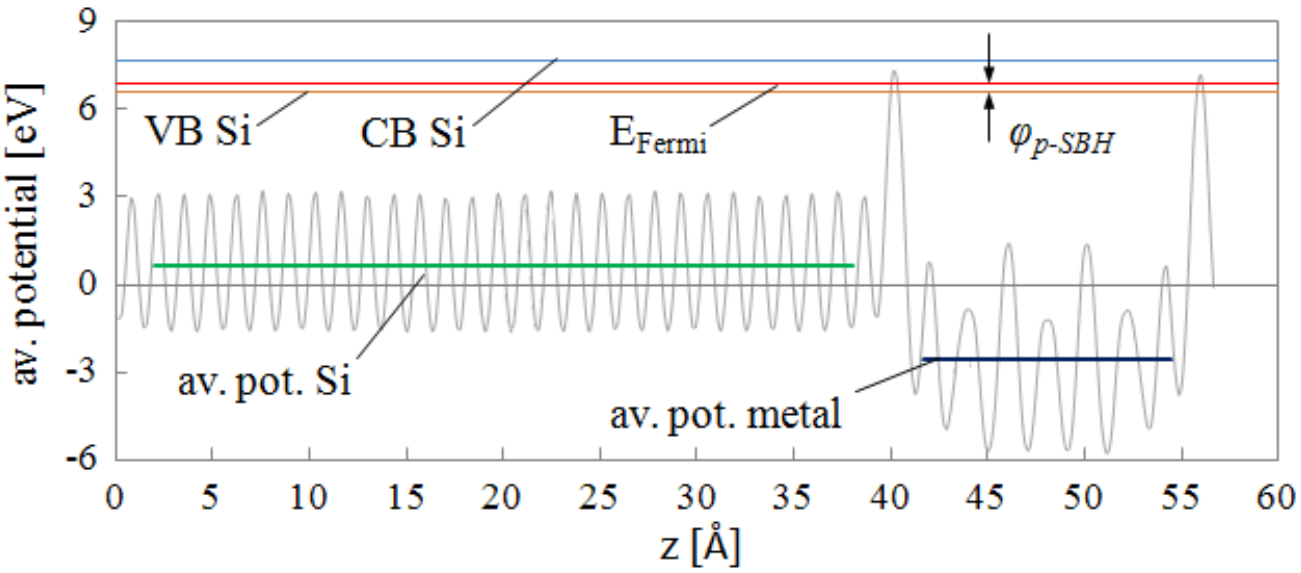

Figure 5b BF11678 19DEC2011

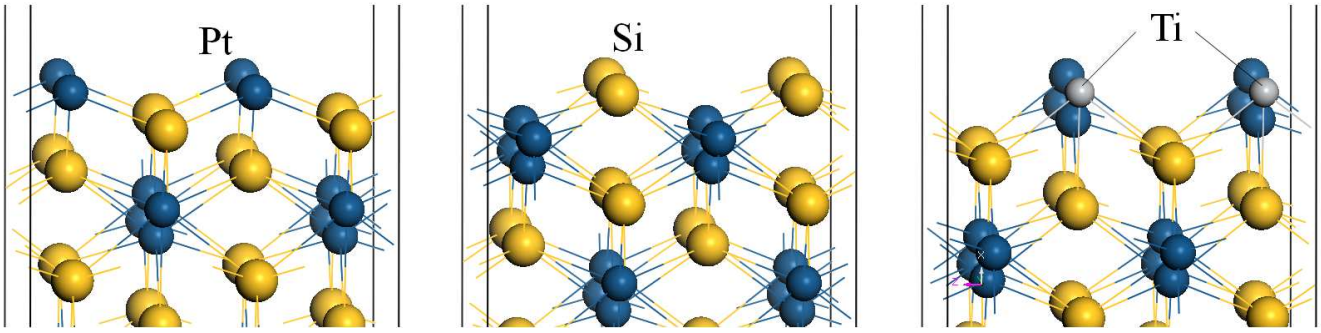

Figure 6 BF11678 19DEC2011

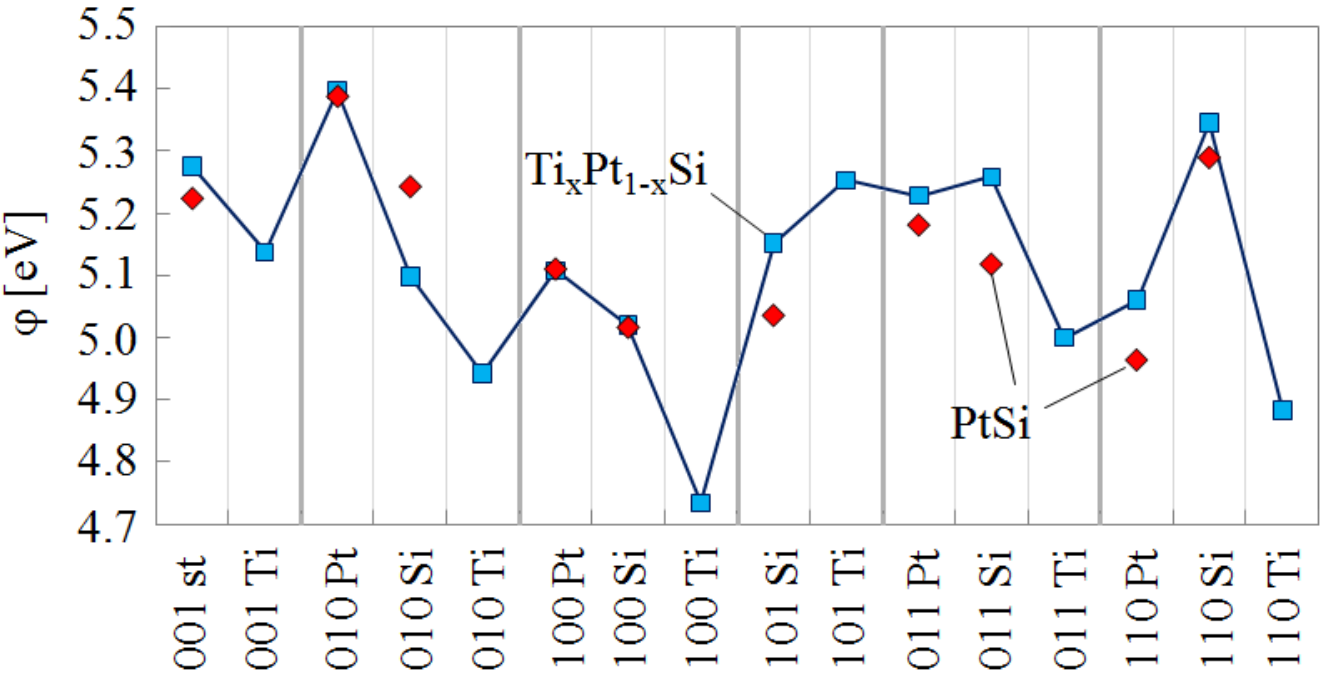

Figure 7 BF11678 19DEC2011

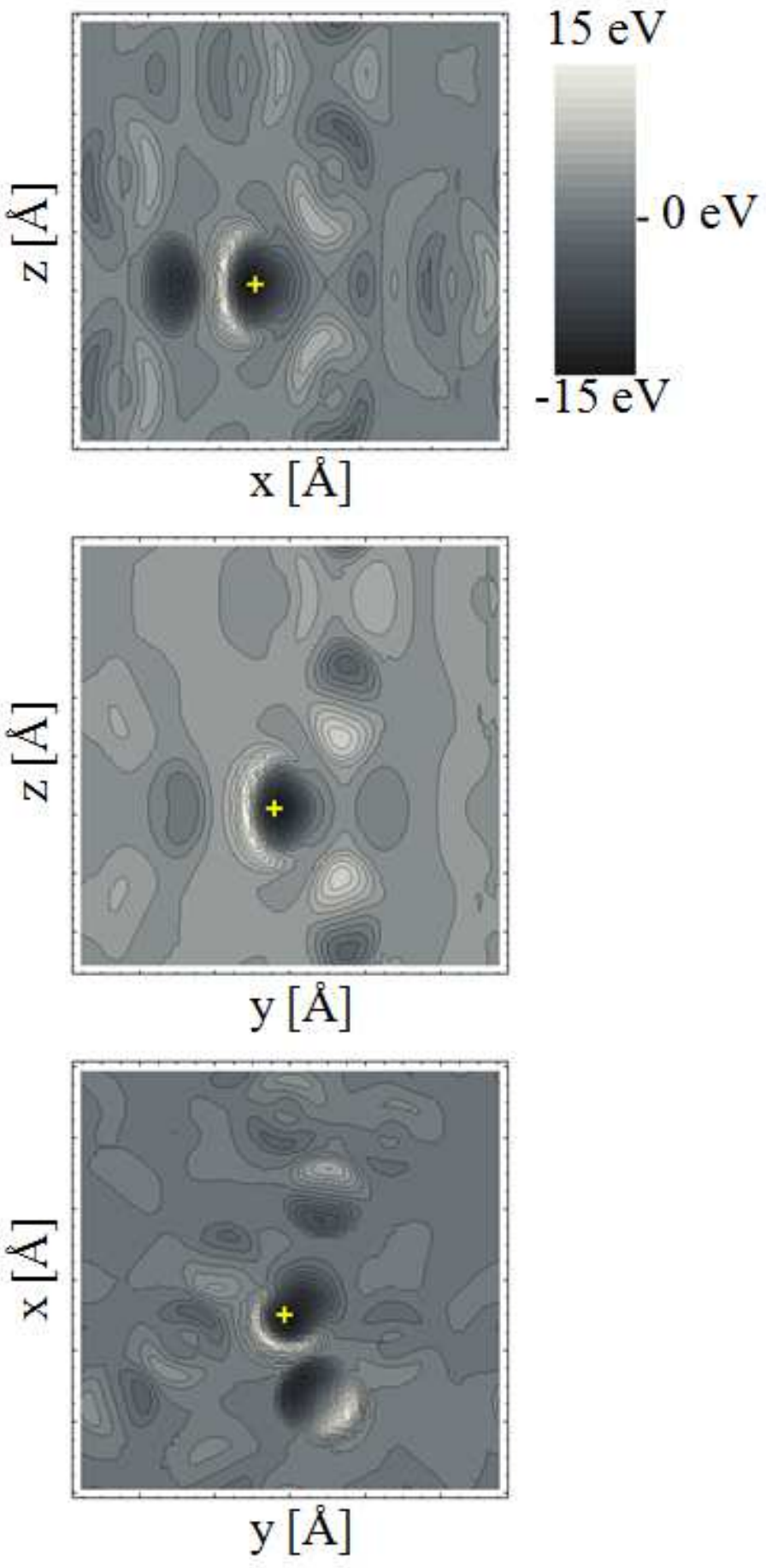

Figure 8 BF11678 19DEC2011

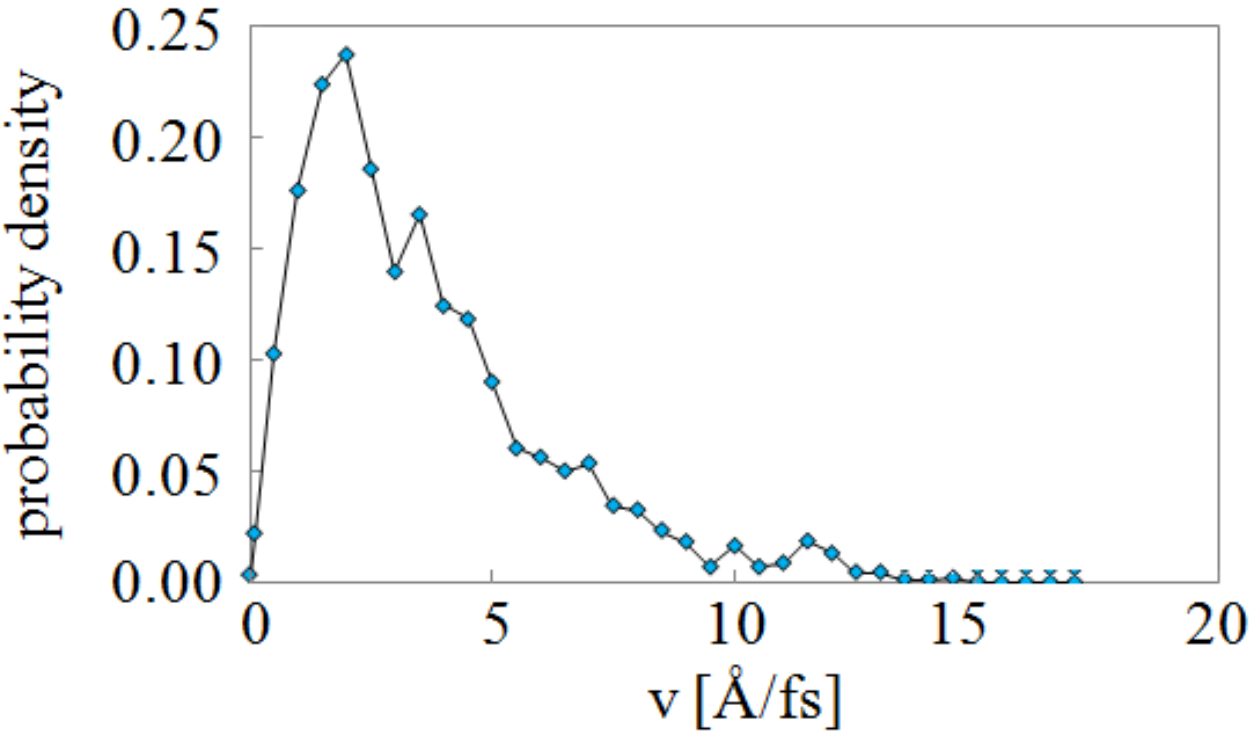

Figure 9 BF11678 19DEC2011

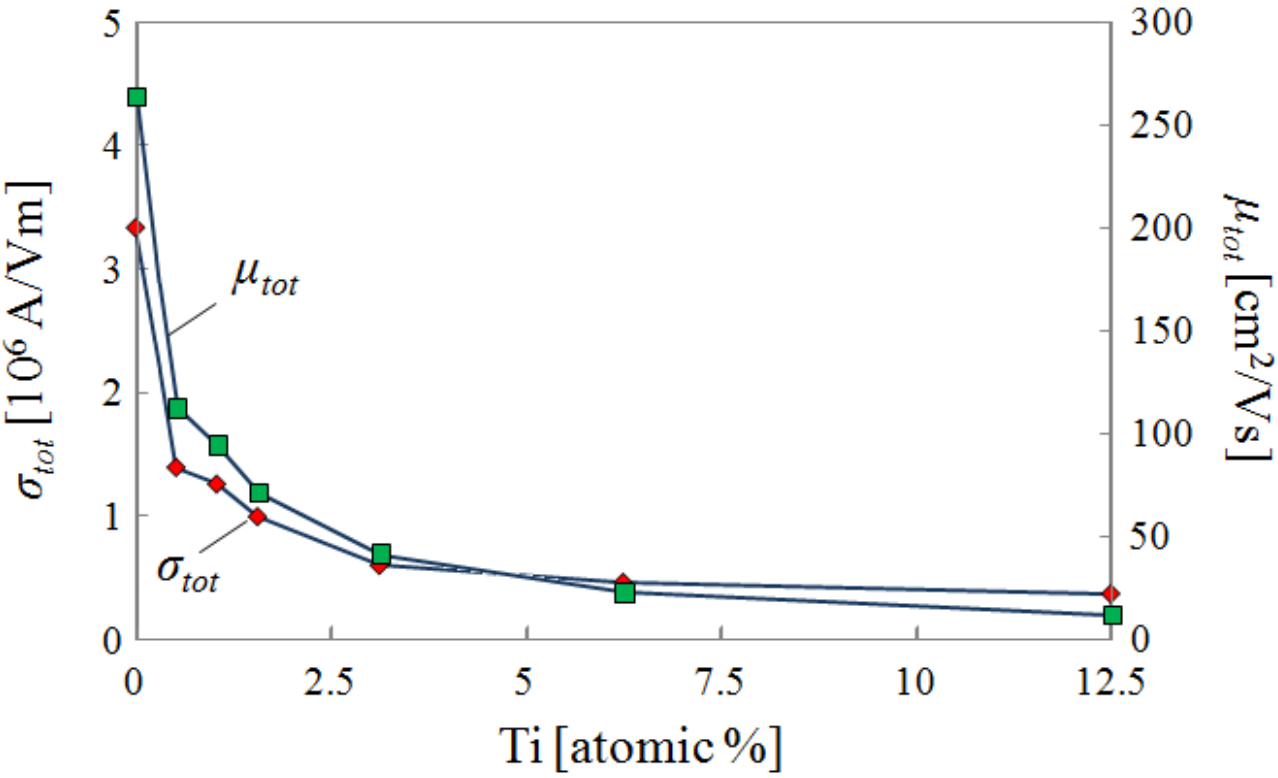

Figure 10 BF11678 19DEC2011

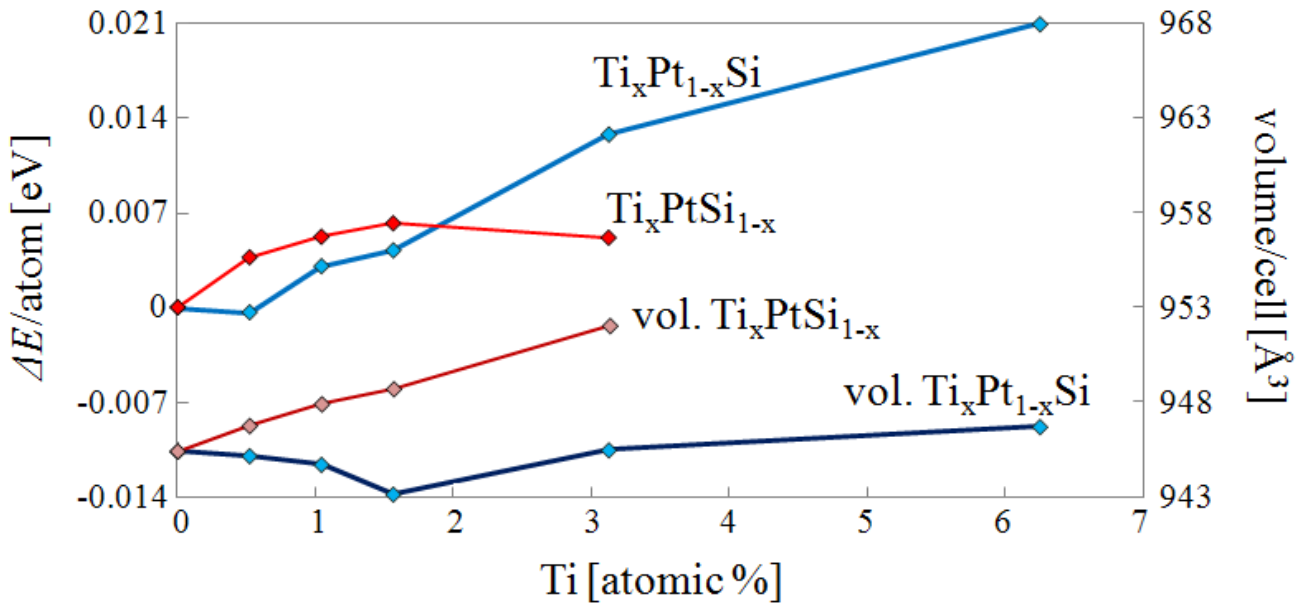

Figure 11 BF11678 19DEC2011

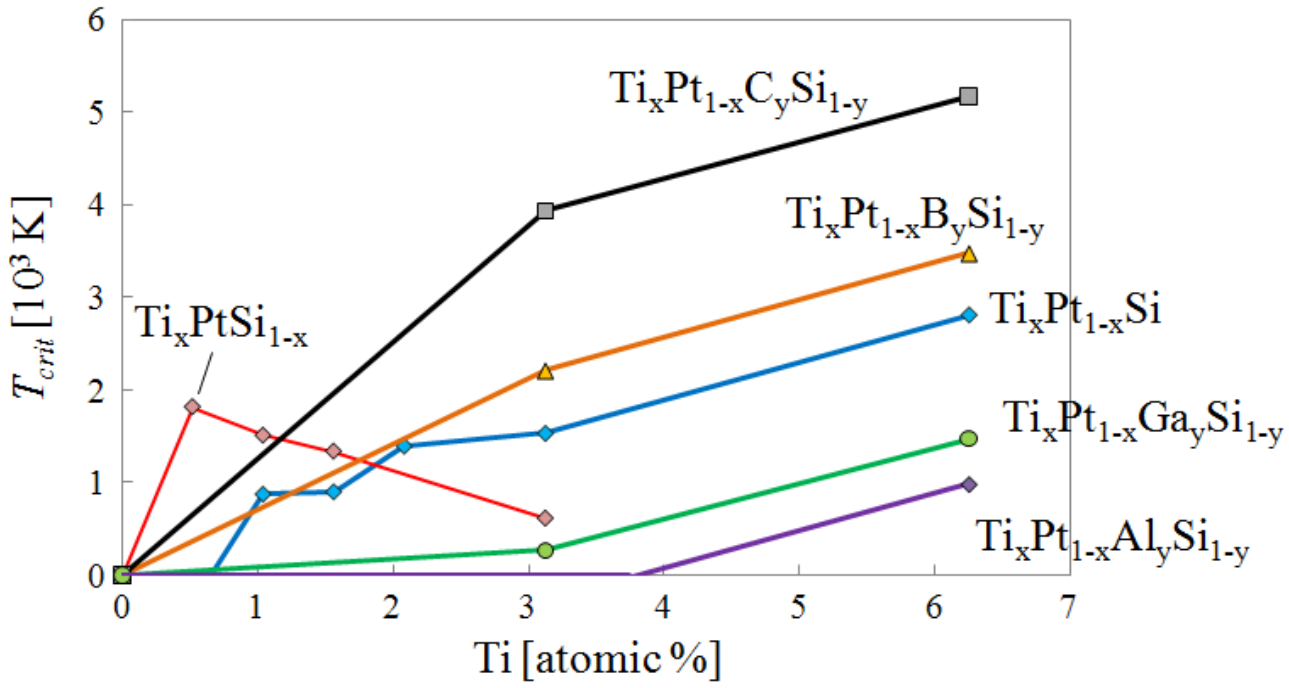

Figure 12 BF11678 19DEC2011